MACE4IR: A foundation model for molecular infrared spectroscopy

Nitik Bhatia[1,2], Ondřej Krejčí[2,3], Silvana Botti[4],
Patrick Rinke[1,2,5,6*], Miguel A. L. Marques[4*]

[1*]Department of Physics, Technical University of Munich,
James-Franck-Strasse 1, Garching, 85748, Germany.
[2]Department of Applied Physics, Aalto University, P.O. Box 11000,
AALTO, FI-00076, Finland.
[3]Department of Mechanical and Materials Engineering, Vesilinnantie 5,
Turku, Finland.
[4*]Research Center Future Energy Materials and Systems of the
University Alliance Ruhr and Interdisciplinary Centre for Advanced
Materials Simulation, Ruhr University, Universitätsstraße 150, Bochum,
D-44801, Germany.
[5]Atomistic Modelling Center, Munich Data Science Institute, Technical
University of Munich, Walther-Von-Dyck Str. 10, Garching, 85748,
Germany.
[6]Munich Center for Machine Learning (MCML), Munich, Germany.

*Corresponding author(s). E-mail(s): patrick.rinke@tum.de;
miguel.marques@rub.de;
Contributing authors: nitik.bhatia@tum.de; ondrej.krejci@utu.fi;
silvana.botti@rub.de;

Abstract

Machine-learned interatomic potentials (MLIPs) have shown significant promise
in predicting infrared spectra with high fidelity. However, the absence of
general-purpose MLIPs capable of handling a wide range of elements and their
combinations has limited their broader applicability. In this work, we introduce
`MACE4IR`, a machine learning foundation model built on the `MACE` architecture
and trained on 10 million geometries and corresponding density-functional theory
(DFT) energies, forces and dipole moments from the QCML dataset. The train-
ing data encompasses approximately 80 elements and a diverse set of molecules,

1

including organic compounds, inorganic species, and metal complexes. `MACE4IR` accurately predicts energies, forces, dipole moments, and infrared spectra at significantly reduced computational cost compared to DFT. By combining generality, accuracy, and efficiency, `MACE4IR` opens the door to rapid and reliable infrared spectra prediction for complex systems across chemistry, biology, and materials science.

1 Introduction

Infrared (IR) spectroscopy is a fundamental technique used to probe the vibrational properties of molecules and materials, offering valuable insight into molecular structures, bonding, and chemical dynamics [1]. IR plays a central role across diverse fields such as catalysis, drug design, environmental chemistry, and materials discovery [1–5]. Accurately predicting IR spectra is crucial for interpreting experimental results, assigning spectral features, and accelerating the discovery and characterization of novel compounds [6–9].

Traditionally, IR spectra predictions have been based on first-principles approaches such as density functional theory (DFT), either within the harmonic approximation [10–12] or through *ab initio* molecular dynamics (AIMD) [12]. Harmonic analysis provides a computationally efficient means of estimating vibrational frequencies and intensities, but it overlooks anharmonicity and temperature-dependent effects, factors that are often essential for accurate spectral interpretation. In contrast, AIMD offers a more realistic representation by simulating vibrational dynamics at finite temperatures, thereby capturing these effects. However, its substantially higher computational demands limit its use to small molecular systems or short simulation timescales [12–14]. These constraints present significant challenges for investigating larger molecules, periodic systems, or performing high-throughput spectroscopic analyses.

Recent developments in machine-learned interatomic potentials (MLIPs) have significantly advanced the field by offering near first-principles accuracy at a fraction of the computational cost [15–24]. Early MLIP frameworks, such as the Behler–Parrinello neural network potentials [15, 25], or kernel-based models like the Gaussian Approximation Potentials (GAPs) [16], demonstrated good accuracy and adaptability across diverse chemical and materials systems. More recently, the emergence of message-passing neural networks, particularly equivariant graph neural networks (GNN) [23, 24, 26–29], has led to notable improvements in data efficiency, predictive accuracy, and model transferability. By embedding rotational and permutational symmetries, these architectures offer more physically grounded representations and generalize better to new chemical environments. Their shared representations and tensor operations also avoid combinatorial scaling with chemical species, thus allowing training highly multi-elemental models [23, 24, 26–30].

Despite rapid progress, most existing MLIPs are tailored to specific systems, such as organic molecules, nanoclusters, bulk crystals, or catalytic surfaces, and are typically trained on expensive DFT datasets curated for those specific applications [7, 26, 31–36]. As a result, they often lack the flexibility to generalize beyond their original domain, limiting their transferability and reuse across different material or molecular systems [33, 35, 37, 38]. In recent years, several initiatives have focused on developing more generalizable MLIPs by training them on large, chemically diverse datasets, with the goal of enhancing their performance across previously unseen chemical environments [29, 39–47]. However, even the most general-purpose MLIPs are seldom developed with vibrational or spectroscopic accuracy in mind. Specifically for IR spectral prediction, which require not only precise force calculations but also accurate dipole moments, widely applicable MLIPs are lacking.

Recently, MLIPs have been extended to predict IR spectra by learning not only energies and forces, but also dipole moments and vibrational properties. This enables both harmonic frequency analysis and molecular dynamics-based spectral simulations [26, 28, 32, 48–59]. However, current MLIPs capable of simulating IR spectra remain limited to narrow chemical domains and have not yet been systematically tested against molecular dynamics-based IR spectra predictions [52, 57, 60–63]. This leaves a clear gap in developing robust, transferable MLIP that can handle diverse molecular families, enabling fast and accurate IR spectral simulations at scale and, therefore, supporting molecular identification from experimental data.

In this work, we address the current lack of a universal MLIP for IR spectroscopy by introducing `MACE4IR`, designed to deliver accurate and efficient IR predictions across a wide chemical space. To establish a stable foundation model, we build on the equivariant message-passing neural network `MACE` [27, 28], which has demonstrated strong performance in both IR property prediction [59] and general-purpose MLIP development [46, 62]. We target the generality of `MACE4IR` across molecular classes, by training on a large-scale dataset of 10 million DFT-calculated geometries from the QCML database [64], spanning around 80 chemical elements.

We assess the robustness of `MACE4IR` by comparing predicted harmonic IR spectra and molecular dynamics-based IR spectra, which capture temperature-dependent anharmonic effects, with reference DFT calculations and experimental data. Testing across diverse molecular families allows us to evaluate the model's transferability. By doing so, we seek to provide the community with the foundation model for high-fidelity spectroscopic applications, usable as-is or adaptable to specific molecules through fine-tuning.

2 Results

We begin by providing an overview of the `MACE4IR` training workflow and evaluations of the trained foundation model, as illustrated in Figure 1. Training starts with a curated subset of the QCML dataset [64], which provides DFT-level energies, forces, and dipole moments. The `MACE4IR` architecture consists of two individual `MACE` models: one for predicting energies and forces (MLIP), and another for dipole moments. Together, these are referred to as the machine learning (ML) model throughout this
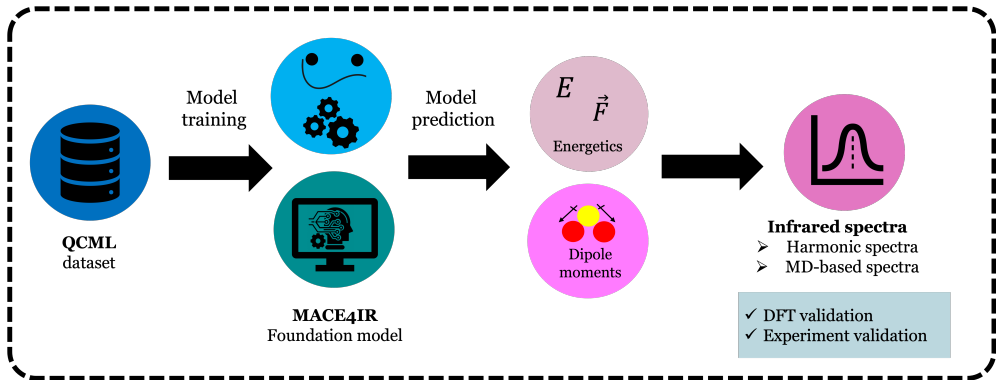
Fig. 1 Illustration of the MACE4IR model development and its performance evaluation in IR spectroscopy. A chemically diverse QCML dataset is used to train the MACE4IR. The resulting model enables accurate and transferable IR spectra predictions using both harmonic and MD-based approach across a broad chemical space, including organic and inorganic molecules, metal complexes, small biomolecules, atmospheric molecules, and various other molecular classes.

work, and are trained to predict the reference properties. Its outputs are either directly compared to DFT calculations or used to simulate IR spectra. Spectra are computed at both the harmonic level and via high-fidelity molecular dynamics (MD) simulations to capture anharmonic, temperature-dependent effects. These predictions are then validated against DFT simulations and experimental spectra for selected molecules. Finally, we assess the model's transferability by applying it to molecules with diverse chemical compositions and structural complexities.

In the following we describe each component of the training workflow and present the results of MACE4IR's comparison to DFT and experimental data.

Training data overview: We use a selected subset of the QCML dataset [64]. The original QCML dataset was constructed by generating conformations from 17.2 million unique chemical graphs, sampled across a wide temperature range (0–1000 K). Initial properties were computed using semi-empirical methods, and a representative set of 33.5 million conformers was subsequently recomputed using DFT to obtain accurate energies, atomic forces, and dipole moments [64]. From this, we retained only neutral molecules with singlet spin multiplicity and randomly selected over 10 million diverse entries spanning approximately 80 elements of the periodic table. For more details on the filtering criteria and data selection, please refer to the Methods section.

The molecules are structurally and chemically diverse and include organic, inorganic, metal complexes and biologically relevant species. This broad coverage is illustrated in Figure 2, which shows the distribution of elements represented in the dataset. While lighter elements such as H, C, N, O, S, and P are most prevalent, reflecting their ubiquity in organic and biochemical molecules, QCML also features molecules with a wide range of heavier main-group and transition metal elements. This broad elemental diversity enable MACE4IR to learn chemically meaningful patterns across
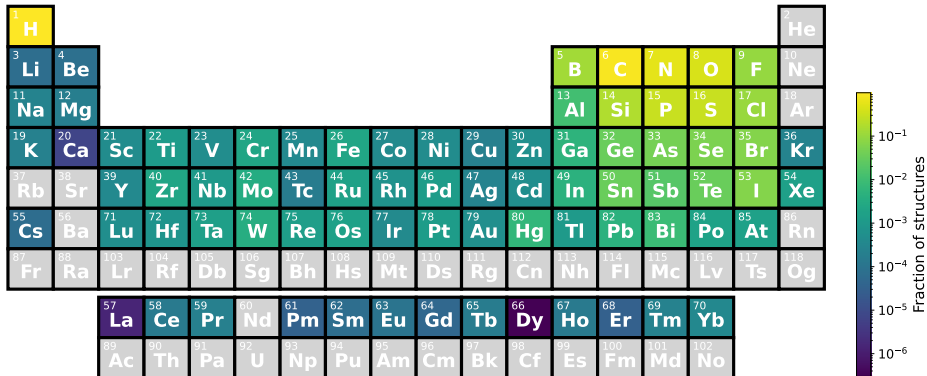
Fig. 2 Elemental distribution in the filtered 10M QCML dataset, highlighting chemical diversity across the periodic table. The color indicates which fraction of structures contains a given element (greyed out entries are not contained in any structure). The majority of structures are composed of H, C, N, O, P, and S, while nearly all elements with atomic number $Z < 86$ are represented in at least a few structures.

varied bonding environments and coordinations, facilitating generalization to complex molecular systems encountered in catalysis, materials science, and environmental applications.

ML model overview: For `MACE4IR`, we employ the `MACE` architecture [27, 28], an equivariant message passing neural network designed to capture complex atomic interactions while respecting the symmetries of physical systems. Specifically, we train two separate models: `MACE-EF`, which predicts total energies and atomic forces in the role of a standard MLIP, and `MACE-D` for predicting dipole moments. Together, these constitute our `MACE4IR` foundation model. The hyperparameters of those models can be found in the Methods section.

ML model training and performance evaluation: To assess how model performance scales with training set size, we implemented a hierarchical training strategy. We prepare subsets of the training data that contain 50k, 100k, 500k, 1M, 3M, 7M, and finally the full dataset of 10M molecular structures. For all training subsets, a fixed set of 100,000 structures was used for validation, and an additional fixed set of 100,000 structures was reserved as the test set for final evaluation. For each training subset, we maintained a consistent model architecture, training one `MACE` model on energies and forces, and a separate model on dipole moments. For the final 10M dataset, we also explored `MACE-EF` models with varying complexity, as detailed in the Methods section. This allowed us to assess trade-offs between model size, training cost, and predictive accuracy.

Model performance was evaluated using the mean absolute error (MAE) for energy, force, and dipole moment predictions. The corresponding performance metrics across all training sizes are summarized in Table 1, with the learning curves shown in Figure 3.

Table 1 Mean absolute errors (MAEs) for energy, force, and dipole moment predictions across different training set sizes on the 100k test set. Energy and force errors are reported for all models; dipole moment errors are shown only for models explicitly trained for dipole prediction. "Small", "Medium", and "Large" refer to the model size (number of parameters). More details can be found in Methods section. The best-performing model, used in all inference tasks, is highlighted in bold.

Training set size	Model size / Precision	Energy (meV/atom)	Force (meV/Å)	Dipole moment (meÅ)
50k	Small / float32	10.7	98.9	41.7
100k	Small / float32	14.1	96.6	36.9
500k	Small / float32	8.1	75.5	29.6
1M	Small / float32	5.1	62.7	26.3
3M	Small / float32	3.8	50.1	25.3
7M	Small / float32	3.4	46.2	23.5
10M	Small / float32	3.3	44.4	**23.3**
10M	Small / float64	3.1	43.9	–
10M	Medium / float32	2.5	32.3	–
10M	Medium / float64	2.3	32.1	–
10M	Large / float64	**2.1**	**30.1**	–

Note: "–" indicates that the dipole moment model was not trained for that configuration.
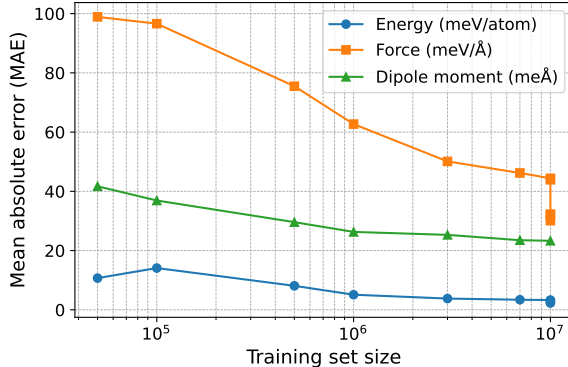

Fig. 3 Mean absolute error (MAE) of energy, force and dipole moment predictions on the test set for the model trained on each given number of examples from the training data.

As expected, we observe a consistent decrease in the prediction error with increasing training data size for all three properties. For the final, large model trained on 10 million molecular structures, we achieve a mean absolute error of 2.1 meV per atom for energy predictions, 30 meV/Å for atomic forces, and 23 meÅ for dipole moment components.

The best performing 10M MACE-EF model (large, float64) was trained in approximately 68.5 hours using 24 AMD MI250x GPUs, while the 10M MACE-D model required around 100 hours on a single AMD MI250x GPU.
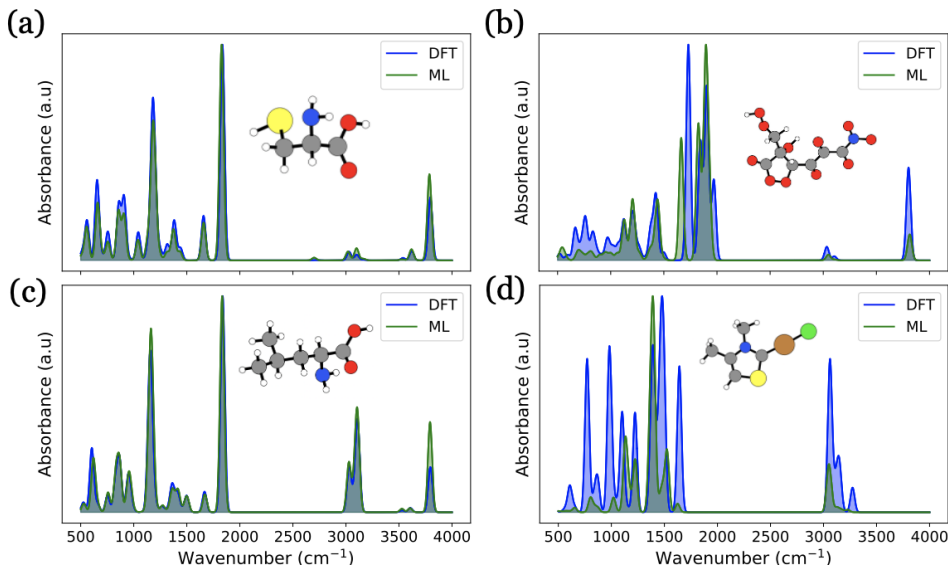
Fig. 4 Comparison of ML-predicted harmonic IR spectra (MACE4IR) with DFT-calculated reference spectra for a representative set of molecules.

Harmonic IR spectra predictions: Next, we tested `MACE4IR` on its ability to predict harmonic IR spectra. We selected a total of 40 molecules, categorized into four distinct chemical classes: organic and inorganic molecules, metal complexes, small biomolecules, and atmospheric species. The organic, inorganic, and atmospheric molecules were selected from the GeckoQ dataset [65], while the metal complexes were taken from the tmQM dataset [66]. Importantly, most of these molecules are not part of the QCML dataset, allowing us to assess the out-of-distribution generalization of the model.

Each class includes 10 molecules that collectively span a wide range of structural and functional diversity, offering a robust benchmark for evaluating the model's generalizability. For each molecule, harmonic vibrational frequencies and intensities were computed with DFT and compared against the corresponding ML predictions. Figure 4 presents harmonic IR spectra for a representative subset of 4 molecules, highlighting the good agreement between the `MACE4IR`-predicted and DFT-computed spectra in terms of peak positions and relative intensities.

To further evaluate the model's performance, we calculated the MAE in vibrational frequencies and intensities for all 40 molecules, using DFT-computed harmonic IR spectra as the reference. On average, the MAE in frequency was found to be 11.58 cm^{-1}, while the MAE in intensity was 0.6580 (D/Å)^2 amu^{-1}, demonstrating the overall reliability of the ML predictions. Among the four chemical classes, the highest prediction errors were observed for metal complex molecules, which exhibited an average frequency MAE of 20.14 cm^{-1} and an intensity MAE of 0.9983 (D/Å)^2 amu^{-1}. In
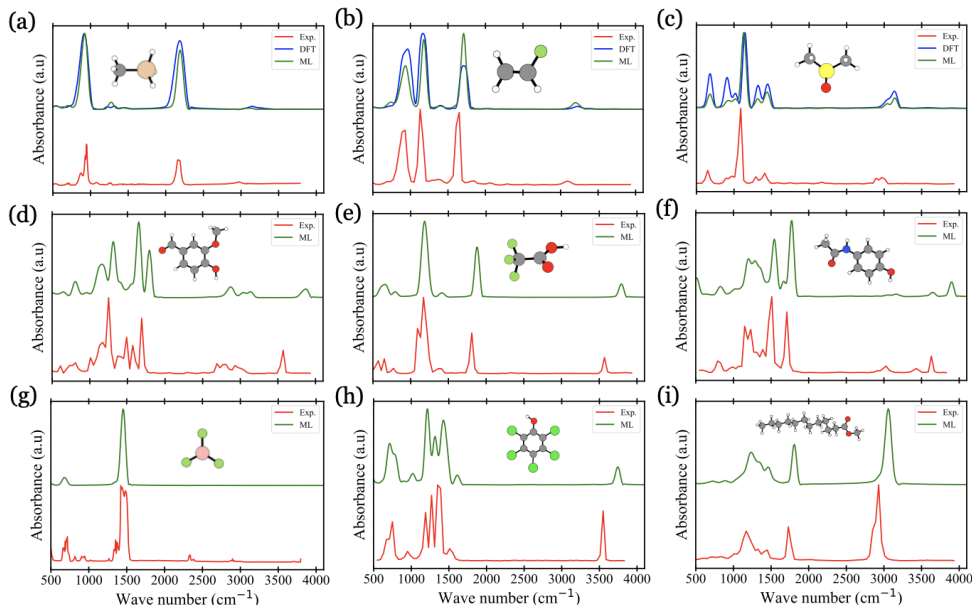
Fig. 5 Comparison of ML-predicted IR spectra with experimental spectra obtained from the NIST database for a diverse set of molecules at 300K: (a) Methylsilane, (b) Fluoroethene, (c) Dimethyl sulfoxide , (d) 4-Hydroxy-3-methoxybenzaldehyde (Vanillin), (e) Trifluoroacetic acid, (f) 4-Acetamidophenol (Paracetamol), (g) Boron trifluoride, (h) Pentachlorophenol, (i) Methyl dodecanoate.

contrast, the lowest errors were obtained for small biomolecules, primarily composed of amino acids, with an average frequency MAE of 3.33 cm^{-1} and intensity MAE of 0.2403 (D/Å)^2 amu^{-1}. Moreover, while DFT-based calculations require $\sim$1,000 CPU hours for a 25-atom molecule, the ML model predicts the spectra in about 2 minutes on a single GPU.

Molecular dynamics based IR spectra predictions: We computed MD-based IR spectra using dipole moment predictions along the MD trajectory at a temperature of 300 K. Further computational details are provided in the Methods section. To assess the performance of `MACE4IR`, we selected 20 molecules from the NIST database [67], each with corresponding experimental IR spectra. Similar to the dataset used for the harmonic spectra calculations, these molecules are not part of the QCML dataset. A representative set of comparisons is presented in Figure 5, illustrating the agreement between the ML-predicted and experimental spectra for 9 diverse molecules. For 3 of these cases, we also performed DFT-based AIMD simulations at 300K to provide a more rigorous comparison; however, due to their high computational cost, such calculations were not feasible for the entire set.

MLMD and experimental spectra agree well in terms of peak positions and intensities, particularly in the lower-frequency region. However, in the higher-frequency range (3000–4000 cm^{-1}), both DFT and MLMD spectra exhibit peak shifts toward higher wavenumbers relative to the experimental spectra. In terms of computational
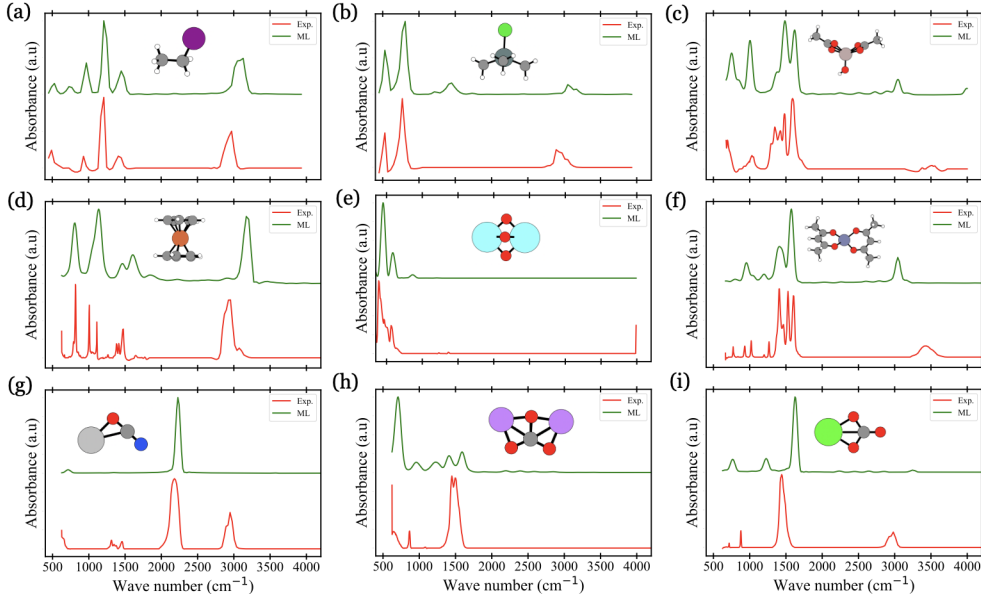
8

Fig. 6 Comparison of ML-predicted IR spectra (MACE4IR) with experimental spectra from the NIST database for a representative set of molecules containing elements with varying frequencies in the training data at 300K: (a) 1-Iodoethane (b) Chlorotrimethylstannane (c) Aluminum diacetate (d) Ferrocene (e) Yttrium oxide (f) Bis(2,4-pentanedionato)zinc (g) Silver cyanate (h) Lithium carbonate (i) Calcium carbonate. The elemental representation in the training dataset gradually decreases from (a) to (i).

efficiency, DFT-based calculations require $\sim$15,000 CPU hours for a molecule comprising 10 atoms, whereas the ML model predicts the spectra in only $\sim$2 hours on a single GPU. The computational cost of MLMD scales linearly with system size, $\mathcal{O}(N)$, in contrast to the quartic scaling, $\mathcal{O}(N^4)$, of DFT calculations with the hybrid PBE0 functional [68].

Assessing generalization over molecules with varying element occurrence: To evaluate how well MACE4IR generalizes, we examined its performance on molecules containing elements with varying frequencies of occurrence in the training data. Instead of limiting our analysis to only the most underrepresented or overrepresented elements (see Figure 2), we curated a diverse set of molecules spanning a broad range of elemental frequencies. These molecules were obtained from the NIST database [67] and are entirely distinct from the QCML dataset used for training, ensuring that this evaluation truly probes the model's extrapolative capabilities. Importantly, this test set is also different from the molecules used in the molecular dynamics-based IR spectra benchmark. This allowed us to examine how well the model captures vibrational features across molecules composed of both common and rare elements.

As shown in Figure 6, the molecules are arranged such that the elemental abundance in the training dataset decreases progressively from (a) to (i). For molecules (a)

9

through (f), which primarily contain elements that are well-represented in the training data, such as main-group elements (H, C, N, O), halogens (Cl, I), metals (Al, Sn), and transition metals like Fe, Zn and Y, the predicted IR spectra align closely with the experimental spectra.

However, for molecules in the last row, (g) silver cyanate, (h) lithium carbonate, and (i) calcium carbonate, the model's predictions deviate more significantly from experimental results. These molecules contain elements (Ag, Li, Ca) that were sparsely represented from the training set. Consequently, the model struggles to accurately capture the corresponding vibrational features, highlighting the limitations of extrapolating to chemical species with low training representation.

3 Discussion

Our study demonstrates the effectiveness of large-scale, equivariant ML model in accurately predicting fundamental molecular properties critical for IR spectroscopy. The MACE4IR model trained on 10 million structures achieved state-of-the-art accuracy across energy, force, and dipole moment predictions, with MAEs of 2.1 meV/atom, 30 meV/Å, and 23 meÅ, respectively. These results underscore not only the precision of the model but also its scalability and robustness across a chemically diverse dataset [64]. Despite the dataset's size and complexity, the model remained computationally tractable: the 10M MACE-EF model completed training in approximately 68.5 hours on 24 AMD MI250x GPUs, while the dipole-predicting MACE-D model required around 100 hours on a single GPU. This highlights the practicality of training foundation-scale models within reasonable computational budgets.

Building on this foundation, we explored the extent to which the model captures both harmonic and anharmonic vibrational features across a range of molecules. The harmonic spectra predictions showed excellent agreement with DFT calculations, with consistently low MAEs across all four chemical classes. Notably, the model achieved the highest accuracy for organic and biomolecular compounds. While the predicted frequencies for metal complexes remained reliable, the intensity values showed relatively larger deviations, pointing to areas for future improvement. These results demonstrate the model's robustness in capturing spectroscopic signatures and its ability to generalize across broad regions of chemical space. A direct comparison with experiment is not provided here, as harmonic spectra typically require the use of an empirical scaling factor to account for anharmonic effects [61], which is beyond the scope of the present study but will be addressed in future work.

The ML model also performs well in predicting MD-based IR spectra, capturing anharmonic effects and finite-temperature spectral broadening with remarkable fidelity (see Figure 5). The predicted spectra show strong agreement with experimental data in terms of both peak positions and relative intensities, particularly in the low-frequency region. However, in the high-frequency range, both DFT- and ML-based spectra exhibit systematic shifts toward higher wavenumbers compared to experimental spectra. This deviation is attributed to the absence of quantum nuclear effects in classical MD simulations, which contributes to the observed discrepancy [50, 69, 70]. Quasi-classical trajectory-based methods, including centroid molecular

dynamics [71] and ring polymer molecular dynamics [72], can capture nuclear quantum effects, but they remain computationally demanding. More sophisticated approaches, such as path-integral coarse-graining simulation [73–75], offer improved agreement by explicitly incorporating quantum nuclear effects into vibrational mode sampling.

We also assessed MACE4IR's ability to generalize across molecules with varying elemental representation in the training data (see Figure 6). While the IR spectra of molecules containing frequently occurring elements (e.g., C, H, N, O, Cl, I, Al, Zn, Fe) were predicted with high fidelity, performance degraded moderately for molecules containing elements that were scarcely represented in the training data, such as Ag, Li, and Ca. Nonetheless, even in these challenging cases, the predicted spectra retained some qualitative agreement with experimental spectra, indicating a degree of generalization beyond the training domain. These findings suggest that performance in such low-representation regions could be further enhanced through fine-tuning or transfer learning strategies. By selectively incorporating additional reference data for underrepresented elements, future models can achieve improved accuracy without the need to retrain from scratch.

Finally, our approach offers a significant advancement in both accuracy and scalability. Traditional methods such as DFT-based AIMD provide high-fidelity IR spectra but are computationally expensive, especially for large systems or long trajectories. In contrast, with our MACE4IR model, spectra can be predicted orders of magnitude faster, reducing computational time from thousands of CPU hours to just minutes or hours on a single GPU, while maintaining comparable accuracy. This efficiency makes it feasible to explore larger systems, longer simulation times, and a broader range of molecular configurations. Recent ML-based approaches have focused primarily on organic molecules or small subsets of chemical space [61, 62]. However, our model generalizes well to broader chemical classes, including metal complexes, organic, inorganic and atmospheric molecules.

With our work, we highlight the potential of ML models to replace or complement traditional quantum chemical calculations in vibrational spectroscopy. This work lays the foundation for future applications such as inverse spectral design, automated reaction monitoring, and integration into high-throughput screening pipelines.

4 Methods

4.1 Machine learning models

In this work, we employ the MACE model [27, 28] for the prediction of total energies, atomic forces, and dipole moments from *ab initio* data. For predicting total energies and atomic forces (MACE-EF), we trained MACE models of varying sizes, characterized by (i) the number of channels (num_channels, defining the dimensionality of node features), (ii) the angular-momentum cutoff (Max_L). MACE represents messages with features labeled by the angular-momentum quantum number L: scalar properties (e.g., total energy) transform as $L = 0$, whereas vectorial properties (e.g., forces, dipole moments) require higher-order ($L > 0$) equivariant features. The distinction

between *"Small"*, *"Medium"*, and *"Large"* models is summarized in Table 2. All models utilized a cutoff radius of 5.0 Å, and two interaction layers, each with a body order of 3. These models were trained using `mace` version 0.3.10.

Table 2 MACE model's parameters trained for energy and force prediction.

Model size	num_channels	Max_L
Small	128	1
Medium	196	1
Large	256	2

In addition to the energy and force models, we trained a separate MACE model to predict molecular dipole moments (MACE-D), which are essential for IR spectral analysis. This model employed (L=1) equivariant messages with a cutoff radius of 5.0 Å, but used a reduced dimensionality of 32 channels to improve efficiency while preserving accuracy. The primary architectural difference lies in the readout layer: instead of summing scalar atomic energies, it outputs a vectorial quantity per atom, which is then summed to obtain the total dipole moment of the molecule.

All training and inference procedures were conducted on AMD MI250x GPUs, ensuring high throughput for large-scale model development and deployment.

4.2 QCML dataset

In this work, we utilize the QCML dataset [64], which represents an initial step toward building a universal quantum chemistry database. The dataset is constructed from 17.2 million unique chemical graphs derived from both known molecular fragments and synthetically generated structures. From these graphs, a total of 14,678 million molecular conformations are sampled across a wide temperature range (0–1000 K), and their properties are initially computed using semi-empirical methods. A randomly selected subset of 33.5 million conformers is then subjected to more accurate quantum mechanical calculations using DFT. This DFT-level dataset includes a wide range of quantum chemical properties, such as total energies, atomic forces, multipole moments, and matrix-based quantities like the Hamiltonian.

The 33.5 million DFT-evaluated conformers span neutral and charged species across various spin multiplicities. For our purposes, we retained only the neutral molecules with a spin multiplicity of 1. We further removed outlier data points from the data set using the flag mentioned in the QCML work. After this filtering, we were left with approximately 15.6 million clean, high-quality DFT structures. Due to computational constraints, we limited the training of our foundation model to a subset of 10 million structures. An additional 100,000 structures each were set aside for validation and test sets, sampled randomly from the remaining data pool.

4.3 DFT computational details

All DFT calculations were performed using the all-electron numeric-atom-centered orbital code FHI-aims [76–79]. The hybrid Perdew-Burke-Ernzerhof exchange-correlation functional (PBE0) [68, 80] was used for the calculations. Further computational settings included the standard FHI-aims tier-2 basis sets and "tight" grid settings, the zeroth-order regular approximation to account for scalar relativistic effects [81]. Structure optimization was carried out using the Broyden–Fletcher–Goldfarb–Shanno (BFGS) minimizer [82], with a convergence limit of 1 meV/Å for the maximum atomic force amplitude. AIMD simulations were performed using the conventional FHI-aims software, while the geometry optimization and harmonic calculations were conducted using the Atomic Simulation Environment (ASE) [83] FHI-aims calculator.

4.4 Harmonic IR spectra calculation

Harmonic IR spectra were computed using the harmonic approximation, where the potential energy surface (PES) is approximated as a quadratic function near the optimized geometry. Vibrational frequencies are obtained by diagonalizing the mass-weighted Hessian matrix of second derivatives with respect to atomic coordinates [10–12]. IR intensities were computed from the derivatives of the molecular dipole moment with respect to mass-weighted normal mode coordinates. The integrated IR absorption intensity A_ν for a normal mode p is given by [12]:

$$A_\nu = \frac{1}{4\pi\varepsilon_0} \frac{N_A \pi}{3c^2} \left(\frac{\partial \boldsymbol{\mu}}{\partial Q_p} \right)^2 ,$$ (1)

where Q_p is the mass-weighted normal coordinate of mode p, $\boldsymbol{\mu}$ is the molecular dipole moment vector, N_A is Avogadro's number, c is the speed of light, and ε_0 is the vacuum permittivity. All calculations of harmonic IR spectra were performed using the ASE calculator and the structures were displaced with 0.002 Å.

4.5 MD simulations

The DFT-based AIMD simulations for IR spectra generation were conducted in two stages. First, the system was equilibrated for 4 ps at the target temperature using the Berendsen thermostat with a relaxation time of 0.1 ps [84]. This was followed by a production run of 50 ps using the Nosé–Hoover thermostat, employing a thermostat mass equivalent to 4000 cm^{-1} [85, 86]. Only the trajectory from the Nosé–Hoover stage was used in the final IR spectra calculations.

All MLMD simulations were performed using a Langevin thermostat [87] with a friction coefficient of 0.01, as implemented in ASE version 3.22.1 [83]. First, 5 ps of each trajectory is used for thermalization, while the following 50 ps are used for the IR simulation.

All MD simulations employed a time step of 0.5 fs, with the temperature maintained at 300 K unless stated otherwise.

4.6 MD simulations-based IR spectra calculation

The IR spectrum is derived from an MD trajectory by evaluating the autocorrelation function of the time derivative of the dipole moment, $\dot{\mu}$. This is expressed as [12]:

$$I_{IR}(\omega) \propto \int_{-\infty}^{+\infty} \langle \dot{\mu}(\tau)\, \dot{\mu}(\tau + t)\rangle_\tau \, e^{-i\omega t} dt. \tag{2}$$

In this work, all auto-correlation functions were computed using the Wiener–Khinchin theorem [88]. To improve the quality of the resulting spectra, a Hann window function [89] and zero-padding were applied prior to the Fourier transform. A maximum correlation time of 1000 fs was used throughout. All spectral processing was carried out using a slightly modified version of the auto-correlation code from SchNetPack [90].

Declarations

The authors report no conflicts of interest. The trained models, scripts, and a tutorial on how to use the models are available in the HuggingFace repository (https://huggingface.co/nitbha007/MACE4IR), while the dataset used for training, the AIMD simulation data, and all input files for the harmonic and MD-based spectra calculations are available on Zenodo (doi: 10.5281/zenodo.16761021 and doi: 10.5281/zenodo.16920067). N.B. created the workflow and proceeded the calculation. O.K., S.B., P.R., and M.M. supervised the work. All authors contributed to the manuscript.

References

[1] Kraack, J.P.: Ultrafast structural molecular dynamics investigated with 2D infrared spectroscopy methods. *Top. Curr. Chem.* **375**(6), 86 (2017)

[2] Haas, J., Mizaikoff, B.: Advances in mid-infrared spectroscopy for chemical analysis. *Annu. Rev. Anal. Chem.* **9**, 45–68 (2016)

[3] Khan, S.A., Khan, S.B., Khan, L.U., Farooq, A., Akhtar, K., Asiri, A.M.: In: Sharma, S.K. (ed.) Fourier Transform Infrared Spectroscopy: Fundamentals and

Application in Functional Groups and Nanomaterials Characterization, pp. 317–344. Springer, Cham (2018)

[4] Zaera, F.: New advances in the use of infrared absorption spectroscopy for the characterization of heterogeneous catalytic reactions. *Chem. Soc. Rev.* **43**, 7624–7663 (2014)

[5] Beć, K.B., Grabska, J., Huck, C.W.: Near-infrared spectroscopy in bio-applications. *Molecules* **25**(12) (2020)

[6] Deglmann, P., Schäfer, A., Lennartz, C.: Application of quantum calculations in the chemical industry—an overview. *Int. J. Quantum Chem.* **115**(3), 107–136 (2015)

[7] Lansford, J.L., Vlachos, D.G.: Infrared spectroscopy data- and physics-driven machine learning for characterizing surface microstructure of complex materials. *Nat. Commun.* **11**(1), 1513 (2020)

[8] Puzzarini, C., Bloino, J., Tasinato, N., Barone, V.: Accuracy and interpretability: The devil and the holy grail. new routes across old boundaries in computational spectroscopy. *Chem. Rev.* **119**(13), 8131–8191 (2019)

[9] Larkin, P.: Infrared and Raman Spectroscopy; Principles and Spectral Interpretation, (2011)

[10] Neugebauer, J., Reiher, M., Kind, C., Hess, B.A.: Quantum chemical calculation of vibrational spectra of large molecules—raman and ir spectra for buckminsterfullerene. *J. Comput. Chem.* **23**(9), 895–910 (2002)

[11] Gussoni, M., Castiglioni, C., Ramos, M.N., Rui, M., Zerbi, G.: Infrared intensities: from intensity parameters to an overall understanding of the spectrum. *J. Mol. Struct.* **224**, 445–470 (1990)

[12] Thomas, M., Brehm, M., Fligg, R., Vöhringer, P., Kirchner, B.: Computing vibrational spectra from ab initio molecular dynamics. *Phys. Chem. Chem. Phys.* **15**, 6608–6622 (2013)

[13] Marx, D., Hutter, J.: Ab Initio Molecular Dynamics: Basic Theory and Advanced Methods. Cambridge University Press, Cambridge (2012)

[14] Gaigeot, M.-P., Spezia, R.: Theoretical Methods for Vibrational Spectroscopy and Collision Induced Dissociation in the Gas Phase, pp. 99–151. Springer, Cham (2015)

[15] Behler, J., Parrinello, M.: Generalized neural-network representation of high-dimensional potential-energy surfaces. *Phys. Rev. Lett.* **98**, 146401 (2007)

[16] Bartók, A.P.: Gaussian Approximation Potentials: The Accuracy of Quantum

15

Mechanics, without the Electrons. *Phys. Rev. Lett.* **104**(13) (2010)

[17] Smith, J.S., Isayev, O., Roitberg, A.E.: ANI-1: an extensible neural network potential with DFT accuracy at force field computational cost. *Chem. Sci.* **8**(4), 3192–3203 (2017)

[18] Gastegger, M., Behler, J., Marquetand, P.: Machine learning molecular dynamics for the simulation of infrared spectra. *Chem. Sci.* **8**(10), 6924–6935 (2017)

[19] Schütt, K.T., Sauceda, H.E., Kindermans, P.-J., Tkatchenko, A., Müller, K.-R.: SchNet – A deep learning architecture for molecules and materials. *J. Chem. Phys.* **148**(24), 241722 (2018)

[20] Zaverkin, V., Kästner, J.: Gaussian moments as physically inspired molecular descriptors for accurate and scalable machine learning potentials. *J. Chem. Theory Comput.* **16**(8), 5410–5421 (2020)

[21] Zaverkin, V., Holzmüller, D., Steinwart, I., Kästner, J.: Fast and sample-efficient interatomic neural network potentials for molecules and materials based on gaussian moments. *J. Chem. Theory Comput.* **17**(10), 6658–6670 (2021)

[22] Deringer, V.L., Bartók, A.P., Bernstein, N., Wilkins, D.M., Ceriotti, M., Csányi, G.: Gaussian process regression for materials and molecules. *Chem. Rev.* **121**(16), 10073–10141 (2021)

[23] Batzner, S., Musaelian, A., Sun, L., Geiger, M., Mailoa, J.P., Kornbluth, M., Molinari, N., Smidt, T.E., Kozinsky, B.: E(3)-equivariant graph neural networks for data-efficient and accurate interatomic potentials. *Nat. Commun.* **13**(1), 2453 (2022)

[24] Musaelian, A., Batzner, S., Johansson, A., Sun, L., Owen, C.J., Kornbluth, M., Kozinsky, B.: Learning local equivariant representations for large-scale atomistic dynamics. *Nat. Commun.* **14**(1), 579 (2023)

[25] Behler, J.: Four Generations of High-Dimensional Neural Network Potentials. *Chem. Rev.* **121**(16), 10037–10072 (2021)

[26] Schütt, K., Unke, O., Gastegger, M.: Equivariant message passing for the prediction of tensorial properties and molecular spectra. In: Meila, M., Zhang, T. (eds.) Proceedings of the 38th International Conference on Machine Learning. Proceedings of Machine Learning Research, vol. 139, pp. 9377–9388. PMLR, ??? (2021). https://proceedings.mlr.press/v139/schutt21a.html

[27] Batatia, I., Batzner, S., Kovács, D.P., Musaelian, A., Simm, G.N.C., Drautz, R., Ortner, C., Kozinsky, B., Csányi, G.: The Design Space of E(3)-Equivariant Atom-Centered Interatomic Potentials (2022). https://doi.org/10.48550/arXiv.2205.06643

[28] Batatia, I., Kovacs, D.P., Simm, G., Ortner, C., Csányi, G.: Mace: Higher order equivariant message passing neural networks for fast and accurate force fields. *Adv. Neural Inf. Process. Syst.* **35**, 11423–11436 (2022)

[29] Bochkarev, A., Lysogorskiy, Y., Drautz, R.: Graph atomic cluster expansion for semilocal interactions beyond equivariant message passing. *Phys. Rev. X* **14**, 021036 (2024)

[30] Drautz, R.: Atomic cluster expansion for accurate and transferable interatomic potentials. *Phys. Rev. B* **99**, 014104 (2019)

[31] Vandermause, J., Xie, Y., Lim, J.S., Owen, C.J., Kozinsky, B.: Active learning of reactive Bayesian force fields applied to heterogeneous catalysis dynamics of H/Pt. *Nat. Commun.* **13**(1), 5183 (2022)

[32] Tang, Z., Bromley, S.T., Hammer, B.: A machine learning potential for simulating infrared spectra of nanosilicate clusters. *J. Chem. Phys.* **158**(22), 224108 (2023)

[33] Ko, T.W., Ong, S.P.: Recent advances and outstanding challenges for machine learning interatomic potentials. *Nat. Comput. Sci.* **3**(12), 998–1000 (2023)

[34] Omranpour, A., Elsner, J., Lausch, K.N., Behler, J.: Machine Learning Potentials for Heterogeneous Catalysis. *ACS Catal.* **15**(3), 1616–1634 (2025)

[35] Olajide, G., Baral, K., Ezendu, S., Soyemi, A., Szilvasi, T.: Application of Machine Learning Interatomic Potentials in Heterogeneous Catalysis. ChemRxiv (2025). https://doi.org/10.26434/chemrxiv-2025-vt9qc

[36] Gurlek, B., Sharma, S., Lazzaroni, P., Rubio, A., Rossi, M.: Accurate Machine Learning Interatomic Potentials for Polyacene Molecular Crystals: Application to Single Molecule Host-Guest Systems (2025). https://arxiv.org/abs/2504.11224

[37] Oca Zapiain, D., Wood, M.A., Lubbers, N., Pereyra, C.Z., Thompson, A.P., Perez, D.: Training data selection for accuracy and transferability of interatomic potentials. *npj Comput. Mater.* **8**(1), 189 (2022)

[38] Kandy, A.K.A., Rossi, K., Raulin-Foissac, A., Laurens, G., Lam, J.: Comparing transferability in neural network approaches and linear models for machine-learning interaction potentials. *Phys. Rev. B* **107**, 174106 (2023)

[39] Chen, C., Ong, S.P.: A universal graph deep learning interatomic potential for the periodic table. *Nat. Comput. Sci.* **2**(11), 718–728 (2022)

[40] Deng, B., Zhong, P., Jun, K., Riebesell, J., Han, K., Bartel, C.J., Ceder, G.: CHGNet: Pretrained universal neural network potential for charge-informed atomistic modeling (2023). https://arxiv.org/abs/2302.14231

[41] Yang, H., Hu, C., Zhou, Y., Liu, X., Shi, Y., Li, J., Li, G., Chen, Z., Chen,

S., Zeni, C., Horton, M., Pinsler, R., Fowler, A., Zügner, D., Xie, T., Smith, J., Sun, L., Wang, Q., Kong, L., Liu, C., Hao, H., Lu, Z.: MatterSim: A Deep Learning Atomistic Model Across Elements, Temperatures and Pressures (2024). https://arxiv.org/abs/2405.04967

[42] Yin, B., Wang, J., Du, W., Wang, P., Ying, P., Jia, H., Zhang, Z., Du, Y., Gomes, C.P., Duan, C., Henkelman, G., Xiao, H.: AlphaNet: Scaling Up Local-frame-based Atomistic Interatomic Potential (2025). https://arxiv.org/abs/2501.07155

[43] Kim, J., Kim, J., Kim, J., Lee, J., Park, Y., Kang, Y., Han, S.: Data-efficient multi-fidelity training for high-fidelity machine learning interatomic potentials (2024). https://arxiv.org/abs/2409.07947

[44] Rhodes, B., Vandenhaute, S., Šimkus, V., Gin, J., Godwin, J., Duignan, T., Neumann, M.: Orb-v3: atomistic simulation at scale (2025). https://arxiv.org/abs/2504.06231

[45] Fu, X., Wood, B.M., Barroso-Luque, L., Levine, D.S., Gao, M., Dzamba, M., Zitnick, C.L.: Learning Smooth and Expressive Interatomic Potentials for Physical Property Prediction (2025). https://arxiv.org/abs/2502.12147

[46] Batatia, I., Benner, P., Chiang, Y., Elena, A.M., Kovács, D.P., Riebesell, J., Advincula, X.R., Asta, M., Avaylon, M., Baldwin, W.J., Berger, F., Bernstein, N., Bhowmik, A., Blau, S.M., Cărare, V., Darby, J.P., De, S., Pia, F.D., Deringer, V.L., Elijošius, R., El-Machachi, Z., Falcioni, F., Fako, E., Ferrari, A.C., Genreith-Schriever, A., George, J., Goodall, R.E.A., Grey, C.P., Grigorev, P., Han, S., Handley, W., Heenen, H.H., Hermansson, K., Holm, C., Jaafar, J., Hofmann, S., Jakob, K.S., Jung, H., Kapil, V., Kaplan, A.D., Karimitari, N., Kermode, J.R., Kroupa, N., Kullgren, J., Kuner, M.C., Kuryla, D., Liepuoniute, G., Margraf, J.T., Magdău, I.-B., Michaelides, A., Moore, J.H., Naik, A.A., Niblett, S.P., Norwood, S.W., O'Neill, N., Ortner, C., Persson, K.A., Reuter, K., Rosen, A.S., Schaaf, L.L., Schran, C., Shi, B.X., Sivonxay, E., Stenczel, T.K., Svahn, V., Sutton, C., Swinburne, T.D., Tilly, J., Oord, C., Varga-Umbrich, E., Vegge, T., Vondrák, M., Wang, Y., Witt, W.C., Zills, F., Csányi, G.: A foundation model for atomistic materials chemistry (2024). https://arxiv.org/abs/2401.00096

[47] Wood, B.M., Dzamba, M., Fu, X., Gao, M., Shuaibi, M., Barroso-Luque, L., Abdelmaqsoud, K., Gharakhanyan, V., Kitchin, J.R., Levine, D.S., Michel, K., Sriram, A., Cohen, T., Das, A., Rizvi, A., Sahoo, S.J., Ulissi, Z.W., Zitnick, C.L.: UMA: A Family of Universal Models for Atoms (2025). https://arxiv.org/abs/2506.23971

[48] Grisafi, A., Wilkins, D.M., Csányi, G., Ceriotti, M.: Symmetry-Adapted Machine Learning for Tensorial Properties of Atomistic Systems. *Phys. Rev. Lett.* **120**(3), 036002 (2018)

[49] Unke, O.T., Meuwly, M.: Physnet: A neural network for predicting energies,

forces, dipole moments, and partial charges. *J. Chem. Theory Comput.* **15**(6), 3678–3693 (2019)

[50] Gastegger, M., Schütt, K.T., Müller, K.-R.: Machine learning of solvent effects on molecular spectra and reactions. *Chem. Sci.* **12**(34), 11473–11483 (2021)

[51] Beckmann, R., Brieuc, F., Schran, C., Marx, D.: Infrared Spectra at Coupled Cluster Accuracy from Neural Network Representations. *J. Chem. Theory Comput.* **18**(9), 5492–5501 (2022)

[52] Zou, Z., Zhang, Y., Liang, L., Wei, M., Leng, J., Jiang, J., Luo, Y., Hu, W.: A deep learning model for predicting selected organic molecular spectra. *Nat. Comput. Sci.* **3**(11), 957–964 (2023)

[53] Stienstra, C.M.K., Hebert, L., Thomas, P., Haack, A., Guo, J., Hopkins, W.S.: Graphormer-IR: Graph Transformers Predict Experimental IR Spectra Using Highly Specialized Attention. *J. Chem. Inf. Model.* **64**(12), 4613–4629 (2024)

[54] Krzyżanowski, M., Matyszczak, G.: Machine learning prediction of organic moieties from the IR spectra, enhanced by additionally using the derivative IR data. *Chem. Pap.* **78**(5), 3149–3173 (2024)

[55] Yuan, M., Zou, Z., Hu, W.: QMe14S, A Comprehensive and Efficient Spectral Dataset for Small Organic Molecules (2025). https://arxiv.org/abs/2501.18876

[56] Cai, Y., Lin, Y., Cai, H., Ni, H.: Deep learning in vibrational spectroscopy: Benefits, limitations, and recent progress. *J. Chin. Chem. Soc.* **72**(6), 611–626 (2025)

[57] Xu, Y., Bian, D., Ju, C.-W., Zhao, F., Xie, P., Wang, Y., Hu, W., Sun, Z., Zhang, J.Z.H., Zhu, T.: Pretrained E(3)-equivariant message-passing neural networks with multi-level representations for organic molecule spectra prediction. *npj Comput. Mater.* **11**(1), 203 (2025)

[58] Falletta, S., Cepellotti, A., Johansson, A., Tan, C.W., Descoteaux, M.L., Musaelian, A., Owen, C.J., Kozinsky, B.: Unified differentiable learning of electric response. *Nat. Commun.* **16**(1), 4031 (2025)

[59] Bhatia, N., Rinke, P., Krejci, O.: Leveraging active learning-enhanced machine-learned interatomic potential for efficient infrared spectra prediction (2025). https://arxiv.org/abs/2506.13486

[60] Zhang, Y., Jiang, B.: Universal machine learning for the response of atomistic systems to external fields. *Nat. Commun.* **14**(1), 6424 (2023)

[61] Pracht, P., Pillai, Y., Kapil, V., Csányi, G., Gönnheimer, N., Vondrák, M., Margraf, J.T., Wales, D.J.: Efficient composite infrared spectroscopy: Combining

the double-harmonic approximation with machine learning potentials. *J. Chem. Theory Comput.* **20**(24), 10986–11004 (2024)

[62] Kovács, D.P., Moore, J.H., Browning, N.J., Batatia, I., Horton, J.T., Pu, Y., Kapil, V., Witt, W.C., Magdău, I.-B., Cole, D.J., Csányi, G.: Mace-off: Short-range transferable machine learning force fields for organic molecules. *J. Am. Chem. Soc.* **147**(21), 17598–17611 (2025)

[63] Kabylda, A., Frank, J.T., Dou, S.S., Khabibrakhmanov, A., Sandonas, L.M., Unke, O.T., Chmiela, S., Müller, K.-R., Tkatchenko, A.: Molecular Simulations with a Pretrained Neural Network and Universal Pairwise Force Fields. ChemRxiv (2025)

[64] Ganscha, S., Unke, O.T., Ahlin, D., Maennel, H., Kashubin, S., Müller, K.-R.: The QCML dataset, Quantum chemistry reference data from 33.5M DFT and 14.7B semi-empirical calculations. *Sci. Data* **12**(1), 406 (2025)

[65] Besel, V., Todorović, M., Kurtén, T., Rinke, P., Vehkamäki, H.: Atomic structures, conformers and thermodynamic properties of 32k atmospheric molecules. *Sci. Data* **10**(1), 450 (2023)

[66] Balcells, D., Skjelstad, B.B.: tmQM Dataset—Quantum Geometries and Properties of 86k Transition Metal Complexes. *J. Chem. Inf. Model.* **60**(12), 6135–6146 (2020)

[67] Wallace, W.E.: NIST Chemistry WebBook, NIST Standard Reference Database Number 69. Linstrom, P. J. and Mallard, W. G.; National Institute of Standards and Technology; Gaithersburg, MD. Vol. 20899, (retrieved September 12, 2024); Chapter "Infrared Spectra" by NIST Mass Spectrometry Data Center. https://doi.org/10.18434/T4D303

[68] Adamo, C., Barone, V.: Toward reliable density functional methods without adjustable parameters: The PBE0 model. *J. Chem. Phys.* **110**(13), 6158–6170 (1999)

[69] Sagiv, L., Hirshberg, B., Gerber, R.B.: Anharmonic vibrational spectroscopy calculations using the *ab initio* CSP method: Applications to H2CO3, (H2CO3)2, H2CO3-H2O and isotopologues. *Chem. Phys.* **514**, 44–54 (2018)

[70] Sauceda, H.E., Vassilev-Galindo, V., Chmiela, S., Müller, K.-R., Tkatchenko, A.: Dynamical strengthening of covalent and non-covalent molecular interactions by nuclear quantum effects at finite temperature. *Nat. Commun.* **12**(1), 442 (2021)

[71] Cao, J., Voth, G.A.: The formulation of quantum statistical mechanics based on the feynman path centroid density. ii. dynamical properties. *J. Chem. Phys.* **100**(7), 5106–5117 (1994)

[72] Craig, I.R., Manolopoulos, D.E.: Quantum statistics and classical mechanics: Real time correlation functions from ring polymer molecular dynamics. *J. Chem. Phys.* **121**(8), 3368–3373 (2004)

[73] Musil, F., Zaporozhets, I., Noé, F., Clementi, C., Kapil, V.: Quantum dynamics using path integral coarse-graining. *J. Chem. Phys.* **157**(18) (2022)

[74] Kapil, V., Wilkins, D.M., Lan, J., Ceriotti, M.: Inexpensive modeling of quantum dynamics using path integral generalized langevin equation thermostats. *J. Chem. Phys.* **152**(12), 124104 (2020)

[75] Kapil, V., Kovács, D.P., Csányi, G., Michaelides, A.: First-principles spectroscopy of aqueous interfaces using machine-learned electronic and quantum nuclear effects. *Faraday Discuss.* **249**, 50–68 (2024)

[76] Blum, V., Gehrke, R., Hanke, F., Havu, P., Havu, V., Ren, X., Reuter, K., Scheffler, M.: Ab initio molecular simulations with numeric atom-centered orbitals. *Comput. Phys. Commun.* **180**(11), 2175–2196 (2009)

[77] Havu, V., Blum, V., Havu, P., Scheffler, M.: Efficient $O(N)$ integration for all-electron electronic structure calculation using numeric basis functions. *J. Comput. Phys.* **228**(22), 8367–8379 (2009)

[78] Ren, X., Rinke, P., Blum, V., Wieferink, J., Tkatchenko, A., Andrea, S., Reuter, K., Blum, V., Scheffler, M.: Resolution-of-identity approach to Hartree-Fock, hybrid density functionals, RPA, MP2, and GW with numeric atom-centered orbital basis functions. *New J. Phys.* **14**, 053020 (2012)

[79] Levchenko, S.V., Ren, X., Wieferink, J., Johanni, R., Rinke, P., Blum, V., Scheffler, M.: Hybrid functionals for large periodic systems in an all-electron, numeric atom-centered basis framework. *Comput. Phys. Commun.* **192**, 60–69 (2015)

[80] Perdew, J.P., Burke, K., Ernzerhof, M.: Generalized gradient approximation made simple. *Phys. Rev. Lett.* **77**, 3865–3868 (1996)

[81] Lenthe, E.v., Baerends, E.J., Snijders, J.G.: Relativistic regular two-component hamiltonians. *J. Chem. Phys.* **99**(6), 4597–4610 (1993)

[82] Nocedal, J., Wright, S.J.: Numerical Optimization. Springer Series in Operations Research and Financial Engineering. Springer, ??? (2006)

[83] Larsen, A.H., Mortensen, J.J., Blomqvist, J., Castelli, I.E., Christensen, R., Dułak, M., Friis, J., Groves, M.N., Hammer, B., Hargus, C., Hermes, E.D., Jennings, P.C., Jensen, P.B., Kermode, J., Kitchin, J.R., Kolsbjerg, E.L., Kubal, J., Kaasbjerg, K., Lysgaard, S., Maronsson, J.B., Maxson, T., Olsen, T., Pastewka, L., Peterson, A., Rostgaard, C., Schiøtz, J., Schütt, O., Strange, M., Thygesen, K.S., Vegge, T., Vilhelmsen, L., Walter, M., Zeng, Z., Jacobsen, K.W.: The

atomic simulation environment—a python library for working with atoms. *J. Phys.: Condens. Matter* **29**(27), 273002 (2017)

[84] Berendsen, H.J.C., Postma, J.P.M., Gunsteren, W.F., DiNola, A., Haak, J.R.: Molecular dynamics with coupling to an external bath. *J. Chem. Phys.* **81**(8), 3684–3690 (1984)

[85] Nosé, S.: A unified formulation of the constant temperature molecular dynamics methods. *J. Chem. Phys.* **81**(1), 511–519 (1984)

[86] Hoover, W.G.: Canonical dynamics: Equilibrium phase-space distributions. *Phys. Rev. A* **31**(3), 1695–1697 (1985)

[87] Ceriotti, M., Bussi, G., Parrinello, M.: Langevin Equation with Colored Noise for Constant-Temperature Molecular Dynamics Simulations. *Phys. Rev. Lett.* **102**(2), 020601 (2009)

[88] Wiener, N.: Generalized harmonic analysis. *Acta Math.* **55**(none), 117–258 (1930)

[89] Blackman, R.B., Tukey, J.W.: The measurement of power spectra from the point of view of communications engineering — Part I. *Bell Syst. Tech. J.* **37**(1), 185–282 (1958)

[90] Schütt, K.T., Kessel, P., Gastegger, M., Nicoli, K.A., Tkatchenko, A., Müller, K.-R.: SchNetPack: A Deep Learning Toolbox For Atomistic Systems. *J. Chem. Theory Comput.* **15**(1), 448–455 (2019)